Master's Thesis of Engineering

Machine Learning-based Prediction of Characteristics of Construction Materials

머신러닝 기반 건설 재료 특성 예측

August 2023

Graduate School of Civil and Environmental Engineering
Seoul National University
Civil and Environmental Engineering Major

Wooyoung Park

Machine Learning-based Prediction of Characteristics of Construction Materials

Jae-Yeol Cho

Submitting a master's thesis of
Civil and Environmental Engineering
August 2023

Graduate School of Civil and Environmental Engineering
Seoul National University
Civil and Environmental Engineering Major

Wooyoung Park

Confirming the master's thesis written by
Wooyoung Park
August 2023

Chair _____(Seal)
Vice Chair _____(Seal)
Examiner _____(Seal)

Abstract

In this study, the several important characteristics of construction materials were successfully predicted using machine learning. Fly ash, as a supplementary cementitious material, has been used to improve the material performance of concrete with cost reduction. Also, carbon nanotubes have recently been added to cementitious materials to implement multi-functionalities of cement-based materials such as self-sensing or self-heating ability. The paper presents machine learning models to predict fly ash's chemical reactivity and carbon nanotubes' dispersion and content. This approach is to find data-driven patterns, unlike traditional theoretical approaches to problem solving.

First, the reactivity of fly ash was predicted by creating a model targeting domestic F-class fly ash, considering the variability of fly ash quality and the difference in reactivity between F-class and C-class fly ash. With a performance of a coefficient of determination of 0.80, the model predicted the content of amorphous aluminosilicate that strongly determines the reactivity of fly ash through the chemical composition of fly ash. Although this model is limited to domestic F-class fly ash, it has a potential for further development to include various types of fly ashes and other types of supplementary cementitious materials which have intrinsically difficulties with regard to characterization as well as quantification of the degree of reactivity.

Second, depending on the dispersion and content of CNTs in cementitious composites, CNTs can improve or worsen the strength

of concrete. Furthermore, intended multi-functionalities due to the inclusion of CNTs in cement-based composites could not be activated. A machine-learning model using computer vision was created to evaluate the quality of CNTs-reinforced concrete non-destructively. The model's accuracy for predicting ultrasonic treatment or the amount of CNTs were very high as 0.92 and 0.89, respectively. This model has practical significance in that it can evaluate the quality of CNT-incorporated cement-based materials, non-destructively. For example, relying on easily obtainable optical microscope images, the content and dispersion of CNT in concrete on the concrete surface could be accurately predicted. The method proposed and validated herein can be also further developed to evaluate other characteristics of construction materials such as porosity or strength prediction which can be implemented as a quality control method of constructed structure.

Keyword : Machine learning, Fly ash, Carbon nanotubes, Ensemble, Convolutional neural network
Student Number : 2021-20672

Table of Contents

Chapter 1. Introduction

1.1. Study Background

Concrete is compatible with other materials, so research is underway to overcome shortcomings by incorporating various chemical admixtures. Typically, there are supplementary cementitious materials (SCMs), which have been proven to reduce CO_2 emissions and improve the overall curing properties of concrete [1]. In addition, research has recently been conducted to improve concrete's mechanical performance and durability by incorporating carbon nanotubes (CNTs) into cement-based materials and to significantly improve electrical conductivity to be used as a smart construction material [2].

It is essential to predict the characteristics of the chemical admixture materials to predict the mechanical performance of concrete and its durability. For example, it is necessary to predict the reactivity of the admixture in the cementitious composites or to check the dispersion and content of the admixture. Typically, the hydration reaction can be analyzed through scanning electron microscope (SEM) photography and X-ray diffraction (XRD) analysis [3-5]. These methods require expensive equipment, and there is a problem that the analysis results vary depending on the

experimental conditions and experimenters. In this context, this study aims to solve these problems using machine learning (ML).

Unlike the conventional theoretical approach, this study finds data patterns composed of input values (x) and target values (y) as a data-driven approach to finding a kind of optimal approximation solution y=f(x). In the case of an artificial neural network model or a deep learning model with a deep layer, it isn't easy to express it as an expression because it has countless parameters, but the approach is the same. Model results can be visualized and analyzed in this case rather than expressions.

1.2. Fly ash

As carbon neutrality has emerged as a global concern, there has been a growing interest in researching SCMs as substitutes for ordinary portland cement [1]. Due to its abundance as an industrial byproduct and its ability to enhance the quality of concrete, FA has become a popular material as an SCM, offering significant economic benefits. However, the quality of FA varies greatly depending on the facilities and operating conditions of coal-fired power plants, and on the types of raw coal [6]. Since the quality of FA has a significant impact on concrete performance [7], it is critical to judge the material properties of FA before being used in cement-based materials.

However, according to ASTM standards, FA is simply classified as C−class or F−class according to only CaO content. Many studies, however, have found that such classifications are inaccurate [8, 9].

FA's reactivity is generally governed by its amorphous phase, because the crystalline phase does not actively participate in the reaction [4, 10]. It is recognized that the component with the greatest reactivity in the amorphous content is aluminosilicate glass, which is a combination of alumina (Al_2O_3) glass and silicate (SiO_2) glass [11−14]. As a result, estimating the quantity of aluminosilicate glass (amorphous aluminosilicate) is critical in predicting the strength of FA contained concrete.

(Song et al, 2021) is first attempt to specify chemical components of FA amorphous phase, which was calculated by the QXRD, through the XRF chemical components of FA using ML [15]. However, considering the number and characteristics of FA data, it seems inappropriate to select the artificial neural network (ANN) algorithm as that study's algorithm. In fact, it has been confirmed that it is difficult to predict for certain F−class FA. The motivation of this study is from the inaccurate prediction result of existing ML model on the FA type F from Korea. FA itself has high complexity and its property (i.e., chemical compatibility with cement−based materials) should be greatly influenced by its geographical origin and the

operational conditions of thermal power plants [16]. Therefore, it is not surprising that the existing ML established based on international database of FA both F and C was not able to accurately predict the reactivity of FA type F from a certain country. Furthermore, it is well known that the hydration mechanism of FA type F and C is different in cementitious materials [17–20]. Therefore, it is rational to separate the type F and C for constructing reliable ML model. This study aims to propose a modified ML to tackle the issue.

1.3. Carbon nanotubes

CNTs possess several key engineering properties, including outstanding Young's modulus of 1000 GPa, high tensile strength of 30 GPa, exceptional current density of 109 A/cm2, and high thermal conductivity of 6000 W/mK [21]. Therefore, CNTs are ideal reinforcing materials for concrete [2, 22]. Incorporating CNTs into concrete significantly enhances its mechanical properties. When a small amount of CNT (0.1%) is added to concrete, the ultimate strain capacity increases by 142%, flexural strength increases by 79%, and fracture toughness increases by 242% [23].

Meanwhile, several authors have reported issues with achieving a homogeneous dispersion of CNTs in cementitious

composites [22−24]. The attraction between particles of CNTs due to Van der Waals forces might be responsible for agglomerations [25]. In general, ultrasonic treatment is used to solve the dispersibility of CNTs [26]. So, the sonication of CNTs is critical to improving the distributed properties of CNTs and concrete performance.

Another thing to consider in improving the concrete strength of CNTs is the amount of CNT. According to [27], when the amount of CNTs added to concrete is less than 0.5 wt.%, the pores in the concrete matrix can be filled by CNT clusters, which reduces the porosity and improves the compactness of the matrix. It enhances the strength of the cement hydration product C−S−H, which significantly contributes to concrete strength. However, when the amount of CNTs added is higher than 0.5 wt.%, the agglomeration of CNTs in the cementitious composites becomes more severe. It causes CNT clusters to dominate the growth space of the hydration product C−S−H, which inhibits the growth of cement hydration product C−S−H in the matrix pores and increases the porosity of the matrix.

In short, the dispersion of CNTs is only secured if sufficient time (5−15min) is allowed during ultrasonic−assisted processing. And the amount of CNT must be appropriately adjusted to efficiently

increase the strength of concrete while the agglomeration of CNTs becomes manageable. Therefore, to use CNTs reinforced concrete in infrastructure facilities, it is essential to check the presence or absence of ultrasonic treatment, which is the most representative dispersion method of CNT, and the amount of CNT.

Here, we propose a time- and cost-effective approach to the maintenance step of CNTs-reinforced concrete using computer vision (CV). This approach is a non-destructive evaluation method. We created a CV-based model to predict the presence or absence of ultrasonic treatment and the amount of CNTs through image data from microscopic equipment that is inexpensive and easy to obtain. Our model predicts whether CNTs powder processing with the ultrasonic method and the amount of CNT (0.05, 0.1, 0.2, 0.4 wt.%) through a microscopic image on the structural surface.

Chapter 2. Materials and Methods

2.1 Reactivity prediction of fly ash type F

2.1.1 Materials and sample preparation

To make an ML model, data is required from which a machine learns and can then test a trained model. The first model was built based on FA from various countries. It will be referred to as model A. As data for model A, 90 FA samples from 13 papers were used [3, 5, 7, 28–37] These papers cover a wide variety of FA from 7 countries. Each FA samples has several features. Features are divided into input and target (output) features. The goal of ML is to derive a data–driven function of input features through given data, and then to predict output features of the test data using only its input features. In model A, each FA sample has six input features and one output feature. Inputs comprise of the chemical composition (wt.%) of six major oxides: (1) Al_2O_3, (2) CaO, (3) Fe_2O_3, (4) SiO_2, (5) MgO, and (6) $Na_2O+0.658K_2O$ (i.e., total alkali content). The output is the aluminosilicate glass content. Fig. 1 shows the distribution of model A dataset.

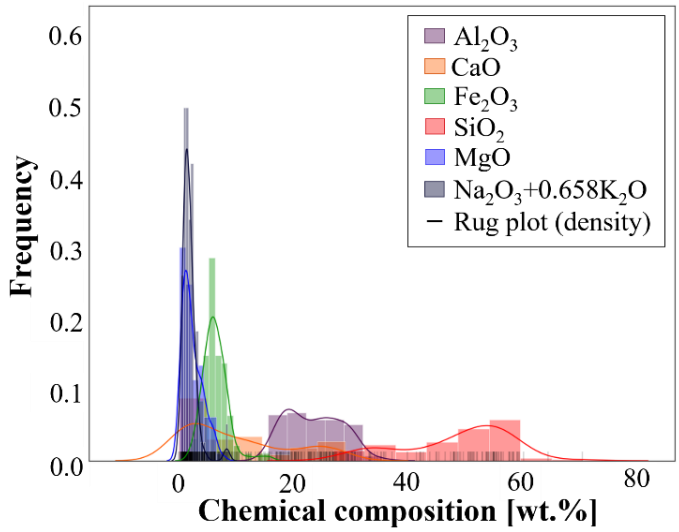

(a) input features (XRF)

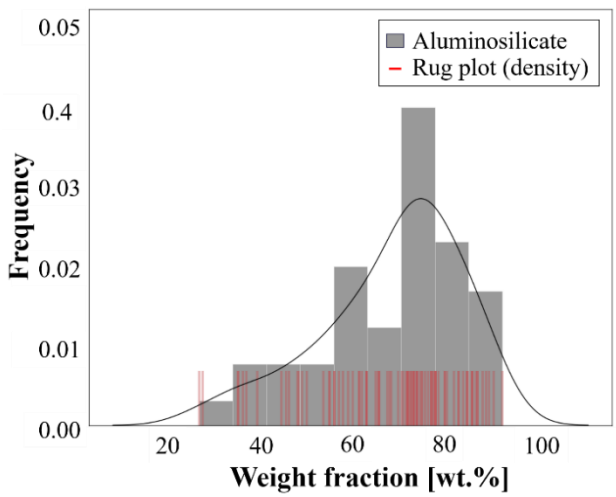

(b) an output feature (QXRD)

Figure 1 Data distribution plot of model A.

Because of the variation in FA both type F and C across countries, the second ML model was made using FA type F from Korea. This will be referred to as model B. As data for model B, 62

FA samples from 17 papers were collected [16, 38–52]. The model B data, like the model A data, comprises the XRF chemical composition of bulk FA as input features, and the amount of aluminosilicate glass determined by QXRD as the output feature. Fig. 2 shows the distribution of model B dataset.

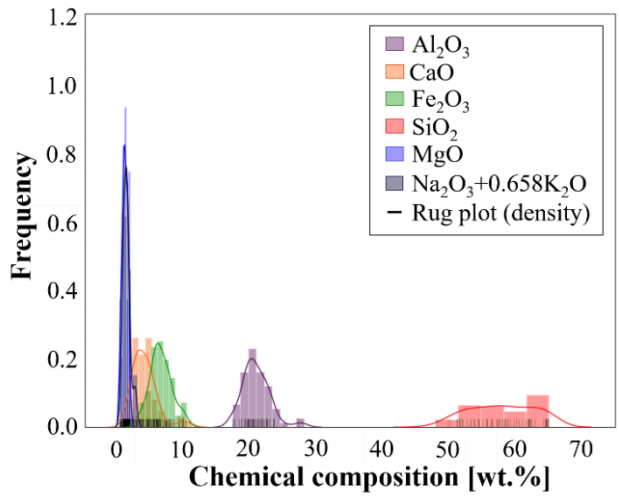

(a) input features (XRF)

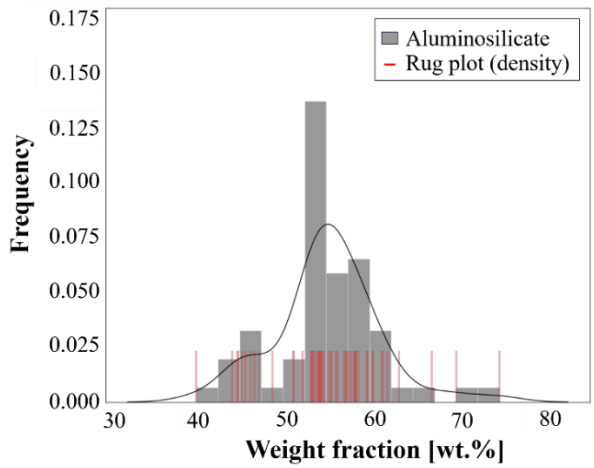

(b) an output feature (QXRD)

Figure 2 Data distribution plot of model B.

But, some of the Korean FA samples in model B dataset cannot predict the target feature. Then, model B dataset has been reconstructed by removing outlier samples. 43 Korean FA types selected from 13 papers were used as data, while 19 FA types were excluded. An ML model has been made as part of the data pre-processing process to determine outliers from the original model B dataset. This model is called the pre-processing model. The pre-processing model used a tree-based ensemble model to prevent biased judgment of outliers for certain models. The description of the outlier(removed) sample and the selected sample determined by the pre-processing model is described in below.

The material property of FA varies considerably, depending on a lot of factors. Even if all input feature values are similar, target feature values can differ drastically if other factors (especially particle size or geographical region) differ from those of typical FA. This can be seen in Fig. 3. The ternary plot consists of network modifiers (i.e., 2Ca+Na+K+2Mg) and two network formers (i.e., Al and Si) as axes. 3-dimension elemental atomic composition of possible network modifiers and network formers are calculated from 6-dimension input features (i.e., chemical composition of XRF). According to the network theory [53], the higher content of network modifiers tend to generate a higher amorphous phase content in

FA[47, 54]. But the ternary plot shows that there is little of this tendency in the used dataset herein. It is considered to be due to different particle size, geographical difference or experimental error that are not included in the input features (but important factors for material property). In this study, these are considered as outliers of type 1. In addition, different ranges of samples among dataset were viewed as type 2 outliers. Thus, 19 samples that cannot be predicted in the pre-processing model are classified as outliers, and the remaining 43 samples are finally used as data for Model B.

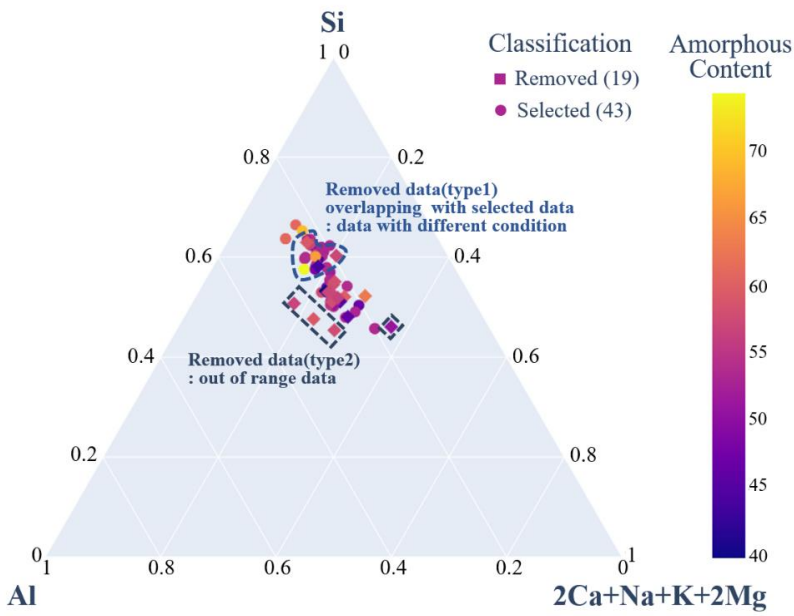

Figure 3 Triangular compositional plot of original model B [atomic %].

2.1.2 Algorithm

Model A was made based on ANN algorithm. The structure of an ANN corresponds to the structure of a biological neural network. The ANN is a network of numerous perceptrons (artificial neurons), as shown in Fig. 4. The ANN procedure is as follows [55]: (1) In the input layer, nodes (i.e., perceptrons) determine whether to consider each input value using the binary variables s_i of each input variables. (2) In the hidden layer, nodes transmit their output value to the posterior nodes when input values from the input layer (or output values of prior nodes, in the case of multiple hidden layers) are multiplied by their synaptic weight w and the result exceeds their threshold θ(bias). The weight represents the impact of the value variation of one node on another. The activation function f(i.e., rectified linear unit, ReLU) is applied in this step. (3) In the output layer, a node yields a target value, which is the output value from the last hidden layer times a synaptic weight. This step is taken by the function g (i.e., linear) instead of the activation function. Steps (1) to (3) of this process are collectively called the "feedforward" approach; this process is a unit of epoch (; iteration). (4) The errors between the target value and the actual value are set as the cost function, and through the derivative of a cost function using chain rule,

the ANN returns to step (1) and repeats the epoch until the error is no longer low and a more appropriate weight and threshold are found. This process is referred as the "backpropagation" approach. Finally, model A was developed using the multiple hidden layer perceptron regressor (MLPRegressor) library, ReLU as an activation function, and MSE as a cost function.

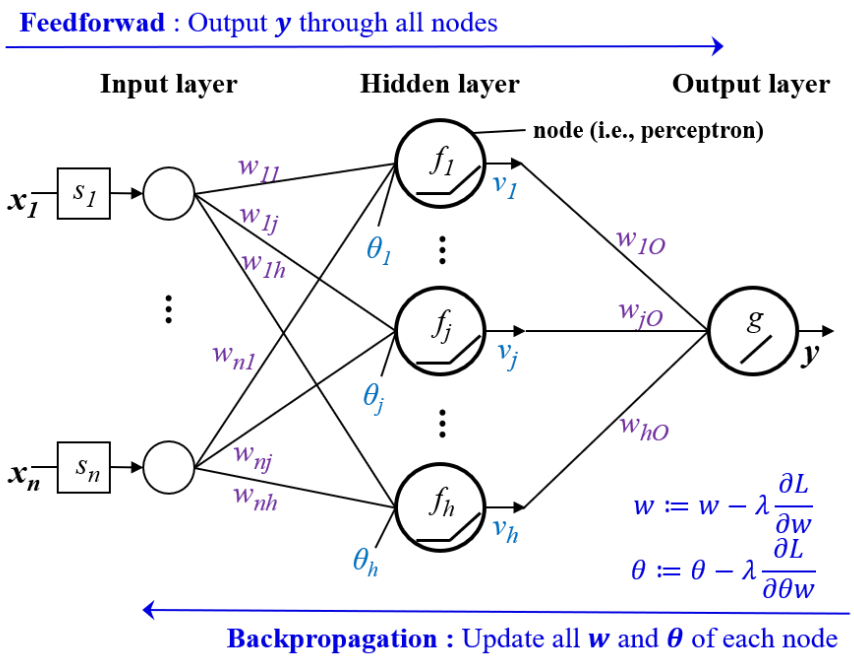

Figure 4 Schematics of ANN [56].

Model A, which corresponds to the preceding study [15], used the ANN model, an inappropriate algorithm, considering the number and characteristics of FA data. The ANN algorithm requires at least hundreds of data [57], and the fly ash data requires more data

because of the large variation. If it learns less than 100 data and has high predictions for test data, it is likely that the given data does not represent the whole data of the world. Therefore, we predicted that model A would not be applied to the F-class FA we collected, and we made it to confirm this. And then, as a solution to this, we created a tree-based ensemble model for F-class FA.

Ensemble algorithm was used in pre-processing model and model B. The ensemble is a multiple learning algorithm. The ANN described above creates one strong learner (optimal model) with a network of numerous perceptrons, while the ensemble method is to create multiple weak learners and synthesizes them to make a more powerful learner. The advantage of this method is that it can solve a trade-off relationship between bias and variance. Bias increases when the model is not sufficiently trained (i.e., underfitting model). On the other hand, variance increases when the model is overlearned and its applicability to new data decreases (i.e., overfitting model) [58]. Therefore, if the bias is lowered, the variance may increase (and vice versa), resulting in a trade-off problem [59]. The best way to solve this problem is to collect and train a lot of data, but it is difficult to obtain a large amount of XRD data of Korean FA. Here, we tried to solve this problem using ensemble algorithms and reveal the

nonlinear structure of the dataset.

Most popular ensembles are boosting, bagging, and stacking ensembles. Fig. 5 shows ensemble algorithm. The purpose of the bagging ensemble is to lower the variance [60]. The boosting ensemble aims to further reduce bias by fitting data, which could not be fitted even through bagging [61]. The stacking ensemble attempted to solve the trade-off problem by blending ensemble models (e.g., bagging and boosting) [59, 62, 63]. In pre-processing model, all three ensembles were used, and model B used one boosting ensemble.

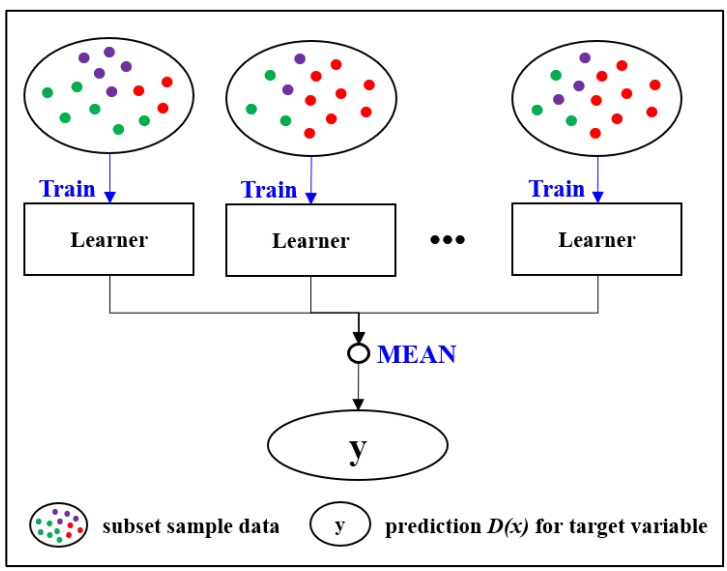

(a) Random forest (bagging) [64]

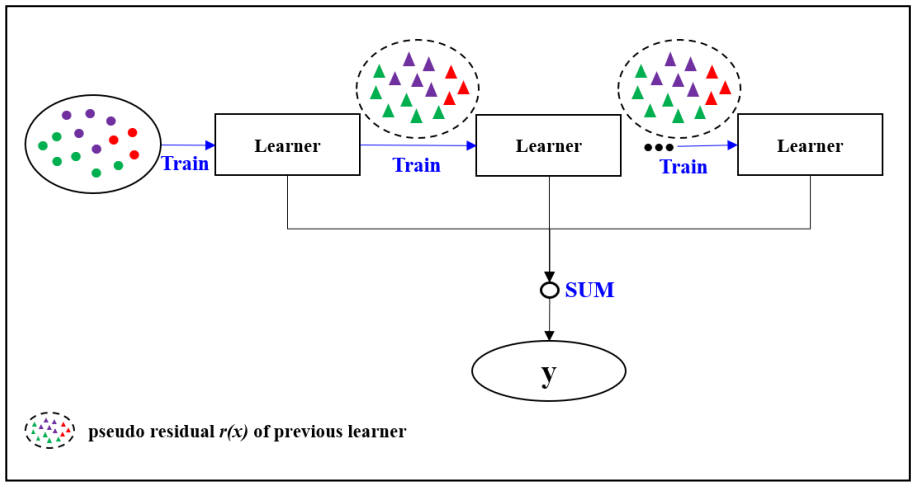

(b) Gradient boosting machine (boosting)

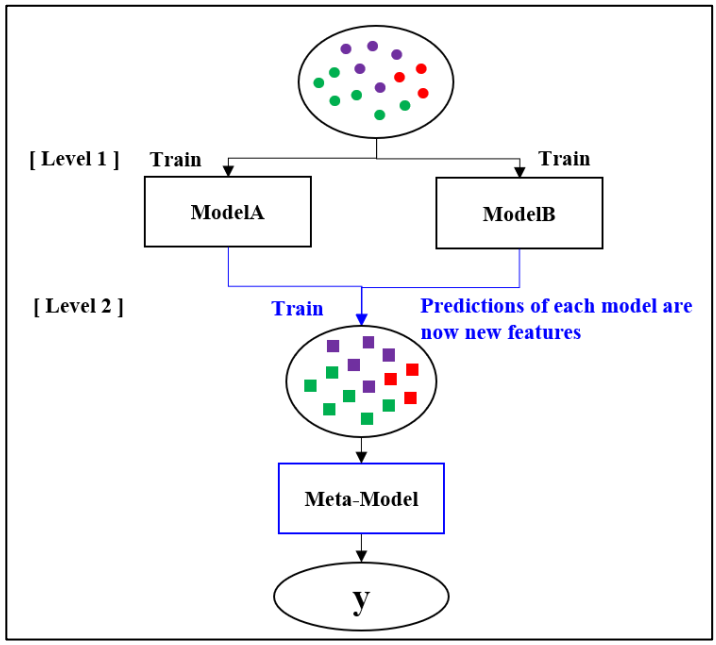

(c) Stacking

Figure 5 Schematics of ensembles : (a) bagging, (b) boosting, and (c) stacking [64] .

2.2 Prediction of characteristics of carbon nanotubes

2.2.1 Materials and sample preparation

The raw materials used for preparing UHPC were white Portland cement (Union cement, Korea), silica fume (Grade 940U, Elkem, Norway), quartz powder (S-SIL 10, SAC, Korea), and silica sand (Saeron, Korea; particle diameters of 0.2–0.3 mm). The chemical composition of raw materials measured via X-ray fluorescence analysis is presented in Table 1. A pellet-type CNT powder (LUCAN BT 1003, LG Chem., Korea) was purchased, and their properties obtained from the manufacturer are listed in Table 3.

The proportion of the CNT/UHPC composite is detailed in Table 3. The water-to-cement ratio and superplasticizer-to-cement ratio were kept at 0.23 and 0.04, respectively. The 0.05, 0.1, 0.2, and 0.4 wt.% of CNTs were mixed with UHPC in two ways: with and without ultrasonication treatment, named with the prefixes S- and N-, respectively. CNT suspensions with ultrasonication were fabricated following the process. The water and CNT powders were placed in a jacketed beaker and dispersed with an ultrasonic processor (Sonoplus, Bandelin, Germany) at a power rate of 2 kJ/min and ultrasonic energy of 350 J/mL. Then, the resulting suspension was stirred with a superplasticizer using a magnetic bar for 10 min.

CNT suspensions without ultrasonication were prepared by placing the water, superplasticizer, and CNT powders in a beaker and magnetically stirring for 10 min at 300 rpm.

Cement, silica fume, quartz powder, and silica sand were blended homogeneously with a Hobert mixer before mixing with CNT suspension for 5 min. Fresh mixtures were placed in cylindrical molds with a height of 20 mm and a diameter of 25 mm. The samples were cured at room temperature and at relative humidity (RH) of 99% in a sealed condition for 24 hours (h). After removing the seal, samples were heat-treated at a temperature of 90 °C and RH of 95% for 48 h. Then, samples were stored under air-drying conditions in a chamber at 20 °C and RH of 60%. Cured samples were cut with diamond blades at 1200 rpm, cleaned with isopropyl alcohol, and dried for 1 h before image acquisition.

Table 1. Chemical compositions of raw materials used (wt.%).

Chemical composition	SiO_2	Al_2O_3	Fe_2O_3	MgO	CaO	K_2O	SO_3	SrO	Loss of ignition	Total
White Portland cement	21.4	4.63	0.358	1.27	65.8	0.13	2.89	0.076	3.4	99.95
Silica fume	96.90	0.29	0.15	0.18	1.54	0.64	–	–	0.02	99.72
Quartz powder	97.70	0.49	0.05	0.21	1.37	0.02	–	–	0.02	99.86

Table 2. Properties of multi-wall CNTs.

Avg. diameter (nm)	Avg. length (μm)	Bulk density (g/cm^3)	Specific surface area (m^2/g)	Purity (wt.%)
13	12	0.12	186	96

Table 3. Mix proportions of CNT/UHPC samples (wt.% of cement).

Samples	Cement	Silica fume	Quartz powder	Silica sand	Water	Superplasticizer	CNT	Dispersion method
S-0.05	1	0.25	0.35	1.1	0.23	0.04	0.05%	Ultrasonication
S-0.1							0.1%	
S-0.2							0.2%	
S-0.4							0.4%	
N-0.05							0.05%	Mechanically stirred
N-0.1							0.1%	
N-0.2							0.2%	
N-0.4							0.4%	

2.2.2 Train and evaluation model

The model is trained using CNN algorithms through a train-dataset (85% of the total dataset). There are two types of target (label) attributes in this study: (1) whether sonication is processed (True or False), and (2) the amount (0.05, 0.1, 0.2, or 0.4 wt.%). The task of simultaneously predicting multiple labels within an image is called multi-label classification. However, without sonication treatment, it is difficult to predict the amount of CNTs because it is not equally dispersed in the cement matrix due to its cohesiveness (Even if the model can expect powder amount, using it isn't very sensible). Therefore, in this study, we confirmed the inaccuracy of the multi-label classification. And we made models individually for each label; this method will be called a parallel classification.

The models' accuracy was visualized using the confusion matrix. A confusion matrix is a powerful tool for visualizing the performance of a model, but simply a confusion matrix is not enough to fully evaluate the performance of a model [65]. Thus, assessing the model's performance more specifically is necessary by performance indicators such as F1-score, Recall, and Precision. The F1-score is calculated as the harmonic mean of precision and recall. It can be obtained using the following equation:

$$F1-score = \frac{2(Precision * Recall)}{Precision + Recall} \quad (1)$$

$$Precision = \frac{TP}{TP+FP}, \qquad Recall = \frac{TP}{TP+FN} \quad (2)$$

In our model, positive refers to the case where sonication treatment is applied (In the case of the CNTs amount problem, each class is assumed to be positive, and Precision, Recall, and F1-score are calculated for each class and then averaged).

The F1-score means the performance of a model considering the balance between Precision and Recall. The Recall is useful when minimizing false negative (FN) is essential, such as in a cancer diagnosis model where it is important not to miss cancer patients. The Precision is useful when minimizing false positive (FP) is key, such as in a spam filtering model where it is essential not to miss important emails [65, 66]. In this model, minimizing FN and FP is necessary, so the F1-score was calculated to measure the final model performance.

Chapter 3. Results and Discussion

3.1 Reactivity prediction of fly ash type F

3.1.1 Model A

Fig. 6(a) shows that obtained R^2 for the train−data is 0.63 for existing database of both fly ash F and C from various countries. R^2 is a metric for measuring how much of a target feature's variation can be predicted from independent variables using a trained model. It normally ranges from 0 to 1. The closer R^2 is to 1, the better the input features can explain the target feature. Model A has an explanatory power of 63%. Not all samples of model A is highly predictable. Therefore, it can be suggested that it is necessary to use an algorithm that is more suitable for the used FA dataset than the ANN algorithm suggested by (Song et al, 2021) [15].

Model A was applied to FA type F from Korea. When accuracy was assessed using 62 types of Korean FA type F as new data, negative value of R^2 was obtained. Negative R^2 means that the prediction accuracy is worse than that predicted by the average. It simply means that the model fits the new data really poorly [67]. It can be a result of biased data used to train the model A. Biased data does not include new data, and the model trained only with such data

are less common. Fig. 6(b) shows that one sample of existing model A database and one Korean sample (12 FA type F) have similar XRF input features, but a QXRD output feature is very different. The quality of FA varies significantly depending on the location of coal-fired power plants, as well as their infrastructure and operational circumstances, and the types of raw coal. Therefore, rather than using FA both type F and C from various countries, it is more economical and accurate to develop an individual model for a specific country in order to uncover the uncertain linkage between the XRF input features and a QXRD target feature of FA, especially considering the high uncertainty that FA material intrinsically has.

To explain the result of model A, Shapley additive explanations (SHAP) analysis is used. The high-dimensional ML model is called a black box model because the exact solution between the input features and the target features is unknown. However, SHAP analysis can quantitatively determine the impact of each input feature on the prediction of a target feature. Fig. 7 shows the SHAP analysis of model A. The SHAP value indicates the importance of each feature based on game theory [68, 69]; Fig. 7(a) is a SHAP value's scatter plot. The horizontal axis represents SHAP values, while the color of the point indicates the value of the feature from low to high. Since the overlapping points are scattered in the y-axis

direction, the distribution of the SHAP values per input feature can be computed. The input features are arranged according to importance. If the SHAP value is negative, this means that it is a factor that lowers the value of a target feature. Positive value indicates that it is a factor that increases the value of a target feature. Fig. 7(b) is a bar plot of the mean of the absolute SHAP value. The larger this value, the more important feature in predicting the target feature. In model A, as the value of CaO, SiO_2, and Al_2O_3 increase, the SHAP value increases, and the impact increases in the negative direction. CaO feature has the highest importance, followed by SiO_2. While Fe_2O_3 and $Na_2O+0.658K_2O$ (i.e., total alkali content) have some impact on the target feature, it is low.

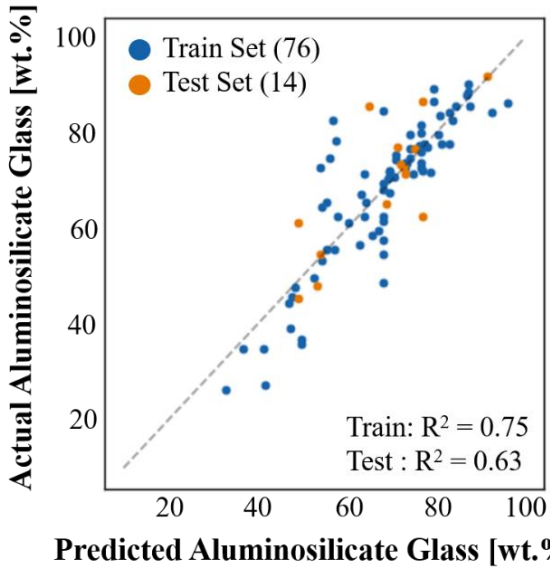

(a) Existing dataset of FA type F and C from various countries

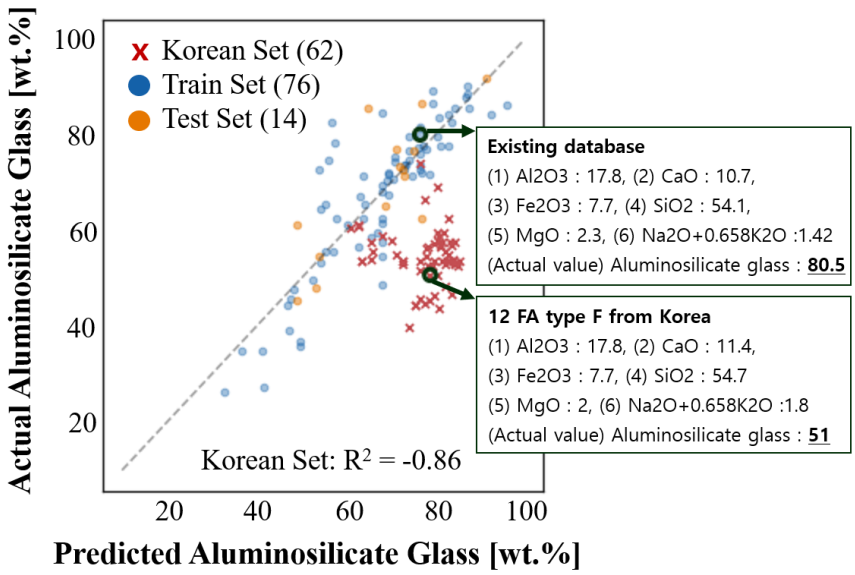

(b) Prediction result of FA type F from Korea

Figure 6 Relationship between prediction and truth of model A.

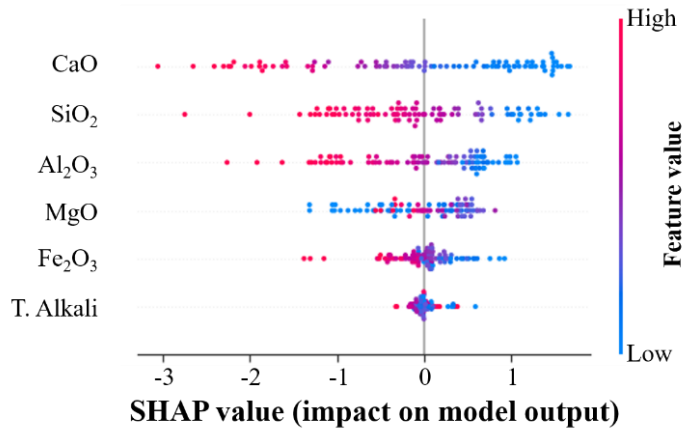

(a) Scatter plot

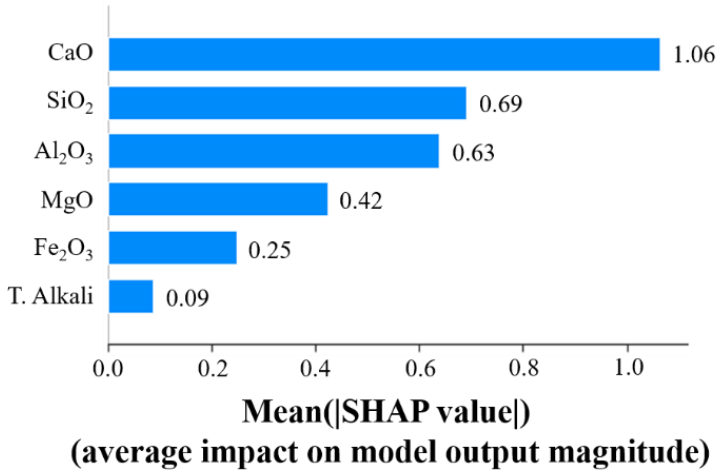

(b) Bar plot

Figure 7 Analysis of the impact of the input features on the target feature in model A.

3.1.2 Model B

For model B, 43 Korean FA type F from 13 papers were chosen as FA samples. Fig. 8 displays the performance of model B. R^2 of the train-data is 0.80; Model B has an explanatory power of 80%. With the exception of a few samples, in most FA samples, aluminosilicate glass content can be precisely predicted from XRF input features.

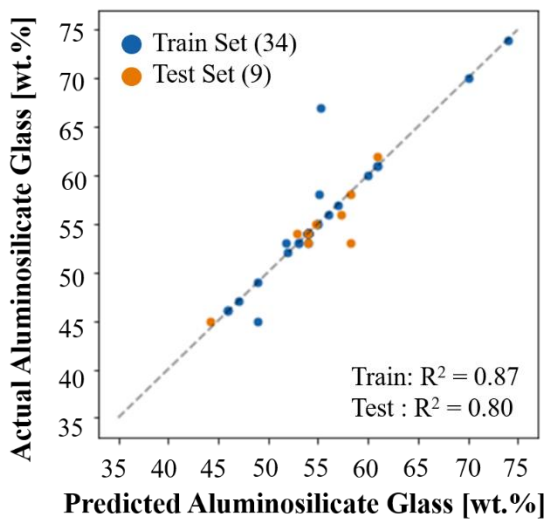

Figure 8 Relationship between prediction and truth of model B.

Fig. 9 shows SHAP analysis of model B. As the value of CaO increases, the SHAP value increases, and the impact increases in the negative direction. CaO feature has the highest importance. While MgO, Fe_2O_3, and $Na_2O+0.658K_2O$ (i.e., total alkali content) have some impact on the target feature, it is low. Therefore, it can be proposed that the refined Model can be applicable to accurately

predict the reactivity of FA type F produced in Korea with high accuracy of prediction.

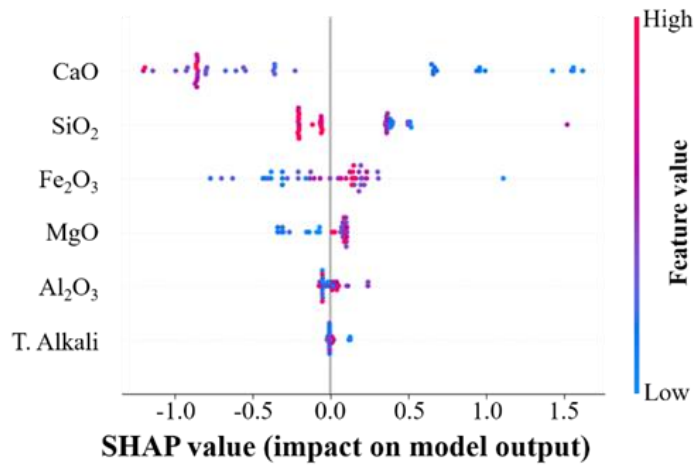

(a) Scatter plot

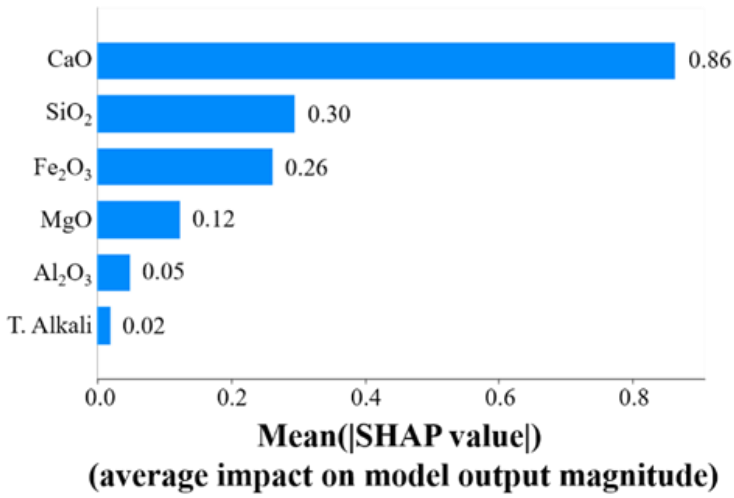

(b) Bar plot

Figure 9 Analysis of the impact of the input features on the target feature in model B.

As a result, when the ML model was individually made only for type F FA from Korea, the prediction accuracy (a coefficient of determination, R^2) is 0.8. As shown in Fig. 10, this is a 27% increase in performance, compared to the existing database of model A. This seems to be because the chemical composition and amorphous phase of FA varies depending on the regions and type (F or C) of FA, which causes the hydration mechanism to be different in cementitious materials. Therefore, it can be concluded that it is more effective and accurate to build ML model considering the specific region and specific type of FA.

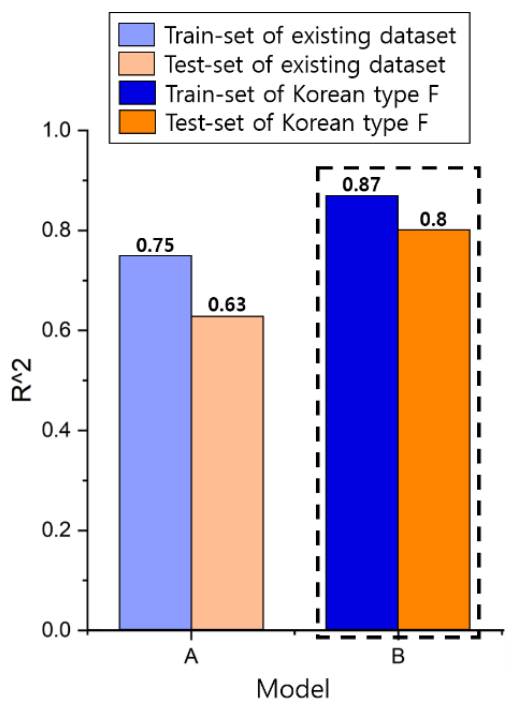

Figure 10 Comparison of prediction accuracy of models A and B.

3.2 Prediction of characteristics of carbon nanotubes

3.2.1 Prediction of whether or not sonication of CNTs

We made CV-based models in parallel for each label. First, we created a model to predict whether sonication is processed. This prediction is binary classification. The data used to train and test the model are for all samples in Table 3. As shown in Fig. 11(a), the model was completed through 100 epochs. Figure 11(b) visualizes the model's accuracy. Based on this, we can calculate performance indicators for the test dataset. Both Accuracy and F1-score are 0.92; that is, this model has high performance.

It shows high accuracy for both the sonication and the non-sonication classes. At low content of 0.05, 0.1, or 0.2 wt.%, ultrasonic treatment can only be distinguished visually, but at 0.4 wt.% amount, it is not easy to distinguish visually. This model is helpful because it can classify whether sonication is processed at any amount of CNTs

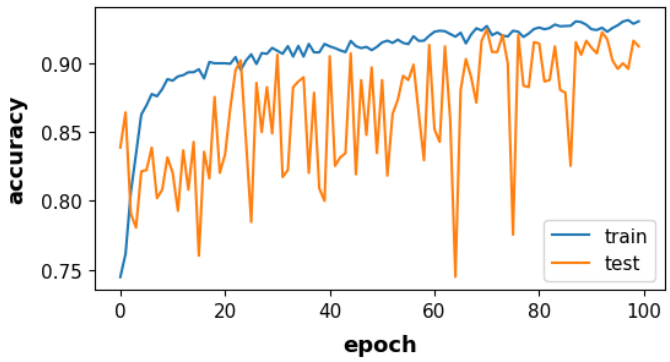

(a) Accuracy

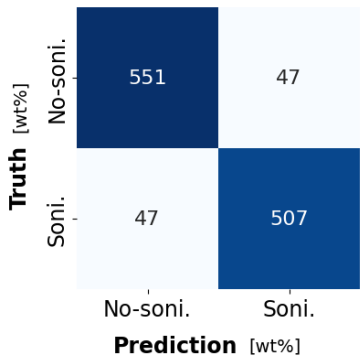

(b) Confusion matrix

Figure 11 Accuracy of prediction of whether or not sonication.

3.2.2 Prediction of content of CNTs

Also, we made a model for predicting the amount of CNTs. The amounts of CNTs in this study consist of 0.05, 0.1, 0.2, and 0.4 wt.%. This task is multiple classification. Since CNTs contents in cementitious composites considered in this study are discrete values, not continuous values, we solve the CNTs amount problem as a classification model, not a regression model. The data used to train

and test the model are for four samples with sonication in Table 3. As shown in Fig. 12(a), the model was completed through 200 epochs. Based on Fig. 12(b), we can calculate performance indicators for the test dataset. The Accuracy and F1−score are 0.89, and this model also has high performance.

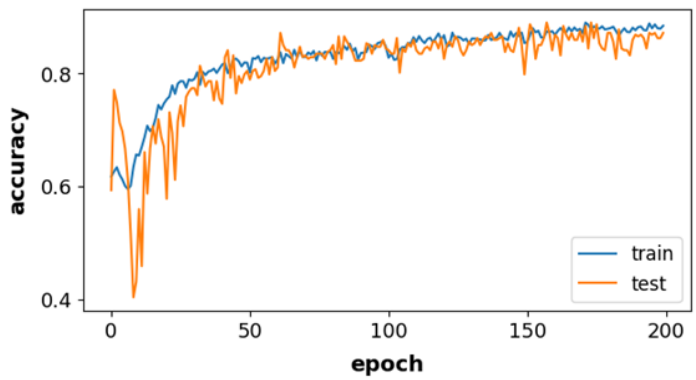

(a) Accuracy

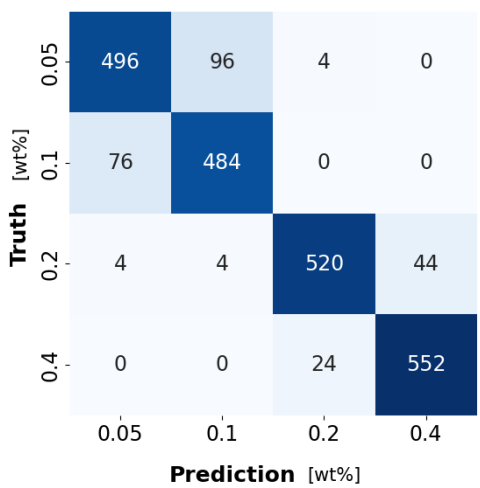

(b) Confusion matrix

Figure 12 Accuracy of prediction of CNTs amount.

As mentioned in Section 2.2.2, when calculating the F1-score of a multi-classification model, assume that each class (CNTs amount) is positive and all remaining classes are negative, calculate Precision and Recall, and then calculate the F1-score by using averaging precision and averaging recall. Recall and Precision for each class are shown in Table 4. At 0.05 and 0.1 wt.%, Recall and Precision are relatively low compared to 0.2 and 0.4 wt.%. Although each class is twice as large as the previous class, the difference between 0.05 and 0.1 classes is as tiny as 0.05%p difference, so the model performance is slightly inferior in classes 0.05 and 0.2 wt.%. However, this indicates that this model is practical in that it accurately predicts content classification that is not easily distinguished visually.

Table 4. Recall and Precision per CNTs amount.

CNTs amount [wt.%]	0.05	0.1	0.2	0.4
Recall	0.83	0.86	0.91	0.9
Precision	0.86	0.83	0.95	0.93

Chapter 4. Conclusion

First of all, this study has achieved mapping XRF chemical composition of the six major oxides into the aluminosilicate glass by refining existing ML model. The most recently proposed model is the ML model for FA type both F and C from various countries. However, this model was not successful in prediction of reactivity of FA type F from Korea. To create an ML model for this specific targeted country, 43 FA type F from Korea were used to develop a final model (i.e., model B) with boosting ensemble algorithm. R^2 (i.e., a score of accuracy) of test-dataset is 0.80. It is possible to predict the amount of aluminum silicate glass of Korean FA using the proposed ML model. Additional conclusions can be drawn from the study are as follows:

1) The model A was built using the ANN algorithm for FA for both F and C collected from various countries of India, Japan, China, the United States, Canada, and Europe. Model A has R^2 of 0.63. However, the amount of aluminosilicate glass was not accurately predicted for the Korean FA type F using this ML model. This result is a negative value of R^2 (0.86), which means that the given model performed even worse than simply predicting the average of the data.

2) The model B has been developed using a boosting ensemble for the selected 43 FAs, excluding the 19 FAs deemed to be outliers. This is the final model of this study, with R^2 of 0.80. As shown in Fig. 8, in most FA samples, the content of the aluminosilicate glass phase is precisely predicted by the chemical composition of the six major oxides obtained by XRF.

3) This study shows that it is possible to predict the aluminosilicate glass content using XRF chemical composition (without the use of QXRD). The ML model of this paper still has the thigs to improve if various quality FA samples are added in the future. This model is a less general model in that it is a model that targets only certain similar quality FA. However, the high accuracy of this ML model is not because unpredictable samples was randomly removed during model optimization, but because similar quality FA was selected through grouping using a pre-processing model before model optimization. In this respect, it is considered that if data of various quality are added, it can be improved to a general model.

4) Nevertheless, as shown in Figs. 7 and 9, it was found that model A and the final model B for Korean FA has

something in common in that CaO content is the most important factor in predicting aluminosilicate glass content, followed by SiO_2 content. And other chemical components also have a meaningful influence. Therefore, this study supports the argument that the ASTM standard for classifying FA considering only CaO content are inaccurate. That is, not only the content of each oxide but also the relationship between each oxide content should be considered. But Al_2O_3 and Fe_2O_3 are ranked differently in models A and B, and there is significant variation in the SHAP values of SiO_2 or lower factors between the two. The obtained different contribution of the elemental composition on the amorphous content can be due to the compositional variance of raw coal.

Second, we developed high-performance computer vision (CV)-based models. These models address two primary issues: predicting whether or not sonication processing and the amount of CNTs. Ensuring the dispersion of CNTs through sonication processing and the control of the CNT content are critical tasks in enhancing the strength and durability of CNTs-reinforced concrete. Further conclusions from this study can be obtained as follows:

1) The first model almost accurately predicts whether

sonication is processed. At a high amount of class (0.4 wt.%) of CNTs, it is challenging to visually distinguish between sonication and non-sonication classes, but this model offers high performance in all classes. The Accuracy and F1-score are 0.92.

2) The second model predicts the amount of CNTs, addressing the balance between increasing concrete strength and managing CNT agglomeration. By dealing with this problem as a multiple classification task, our model can check the content of CNTs in concrete. to be added to concrete. The Accuracy and F1-score are 0.89. This model is slightly inferior to the first-label model. This is considered to be because the difference between classes of 0.05 and 0.1 is small at 0.05%p, making it relatively difficult to distinguish.

3) Our CV-based model enables a non-destructive, time- and cost-effective approach to CNTs-reinforced concrete maintenance. By predicting whether or not sonication processing and content of CNT through image data from inexpensive and readily available optical microscope equipment, our models offer a practical solution to some of the most pressing challenges in the

use of CNTs in cementitious composites. This study underscores the potential of machine learning applications in advancing quality control in material processing and analysis. Future work could continue to harness this predictive power in broader tasks and diverse material types to push the boundaries of construction materials further.

Bibliography

[1] J.M. Paris, J.G. Roessler, C.C. Ferraro, H.D. DeFord, T.G. Townsend, A review of waste products utilized as supplements to Portland cement in concrete, Journal of Cleaner Production 121 (2016) 1-18.
[2] M. Safiuddin, M. Gonzalez, J. Cao, S.L. Tighe, State-of-the-art report on use of nano-materials in concrete, International Journal of Pavement Engineering 15 (2014) 940-949.
[3] P.T. Durdziński, C.F. Dunant, M.B. Haha, K.L. Scrivener, A new quantification method based on SEM-EDS to assess fly ash composition and study the reaction of its individual components in hydrating cement paste, Cement and Concrete Research 73 (2015) 111-122.
[4] R.P. Williams, A. van Riessen, Determination of the reactive component of fly ashes for geopolymer production using XRF and XRD, Fuel 89(12) (2010) 3683-3692.
[5] S.M.A. G. V. P. Bhagath Singh, M.A. Kolluru V. L. Subramaniam, Quantitative XRD Analysis of Binary Blends of Siliceous Fly Ash and Hydrated Cement, The American Society of Civil Engineers (2016).
[6] G. Xu, X. Shi, Characteristics and applications of fly ash as a sustainable construction material: A state-of-the-art review, Resources, Conservation and Recycling 136 (2018) 95-109.
[7] R.T. Chancey, P. Stutzman, M.C.G. Juenger, D.W. Fowler, Comprehensive phase characterization of crystalline and amorphous phases of a Class F fly ash, Cement and Concrete Research 40(1) (2010) 146-156.
[8] C.H. James, M. Maria, An Approach toward a Combined Scheme for the Petrographic Classification of Fly Ash, Energy & Fuels 15 (2001).
[9] A.B. Göktepe, A. Sezer, G.İ. Sezer, K. Ramyar, Classification of time-dependent unconfined strength of fly ash treated clay, Construction and Building Materials 22(4) (2008) 675-683.
[10] C. Ward, D. French, Determination of glass content and estimation of glass composition in fly ash using quantitative X-ray diffractometry, Fuel 85(16) (2006) 2268-2277.
[11] H. Pietersen, A. Fraay, J. Bijen, Reactivity of fly ash at high pH, in fly ash and coal conversion by-products: Characterization, utilization and disposal VI, Materials research society symposium proceedings. Materials Research Society, 1989.

[12] H.J.H. Brouwers, R.J. Van Eijk, Fly ash reactivity: Extension and application of a shrinking core model and thermodynamic approach, Journal of Materials Science 37 (2002).
[13] J.S.J. Sindhunata, G.C. van Deventer, H.X. Lukey, Effect of Curing Temperature and Silicate Concentration on Fly-Ash-Based Geopolymerization, Industrial & Engineering Chemistry 45 (2006).
[14] M. Moomen, C. Siddiqui, Probabilistic deterioration modeling of bridge component condition with random effects, Journal of Structural Integrity and Maintenance 7(3) (2022) 151-160.
[15] Y. Song, K. Yang, J. Chen, K. Wang, G. Sant, M. Bauchy, Machine Learning Enables Rapid Screening of Reactive Fly Ashes Based on Their Network Topology, ACS Sustainable Chemistry & Engineering 9(7) (2021) 2639-2650.
[16] Y.K. Cho, K.M. Lee, Effect of chemical properties of fly ash on the compressive strength of geopolymer, (2019).
[17] C.S. Shon, Testing the Effectiveness of Class C and Class F Fly Ash in Controlling Expansion due to Alkali-Silica Reaction Using Modified ASTM C 1260 Test Method, Journal of Materials in Civil Engineering 16(1) (2004).
[18] M. Sumer, Compressive strength and sulfate resistance properties of concretes containing Class F and Class C fly ashes, Construction and Building Materials 34 (2012) 531-536.
[19] A. Wardhono, Comparison Study of Class F and Class C Fly Ashes as Cement Replacement Material on
Strength Development of Non-Cement Mortar, Materials Science ans Engineering 288 (2017).
[20] I.-S. Yoon, C. Chang, J.-W. Nam, Effect of carbonation on chloride transportation parameters in cementitious materials, Journal of Structural Integrity and Maintenance 7(3) (2022) 161-167.
[21] M.F. Ashby, P.J. Ferreira, D.L. Schodek, Nanomaterials, nanotechnologies and design: an introduction for engineers and architects, Elsevier Science Ltd., Boston, MA, 2009.
[22] N.R.C.o. Canada, The effect of SWCNT and other nanomaterials on cement hydration and reinforcement, NRCC Research Report, 2013.
[23] K.A.A. Rashid, Nanotechnology-based system for damage-resistant concrete pavements, Texas, 2012.
[24] C. Gay, F. Sanchez, Performance of carbon nanofiber -cement composites with a high-range water reducer, Journal of the Transportation Research Board 2142 (2010) 109-113.
[25] L.I. Nasibulina, I.V. Anoshkin, S.D. Shandakov, E.I. Kauppinen, Direct synthesis of carbon nanofibers on cement particles, Journal of the Transportation Research Board 2142(1) (2010) 96-101.

[26] M. Jung, Y.-s. Lee, S.-G. Honga, J. Moon, Carbon nanotubes (CNTs) in ultra-high performance concrete (UHPC): Dispersion, mechanical properties, and electromagnetic interference (EMI) shielding effectiveness (SE), Cement and Concrete Research 131 (2020).
[27] Y. Yao, H. Lu, Mechanical properties and failure mechanism of carbon nanotube concrete at high temperatures, Construction and Building Materials 297 (2021).
[28] T. Oey, J. Timmons, P. Stutzman, J.W. Bullard, M. Balonis, M. Bauchy, G. Sant, An improved basis for characterizing the suitability of fly ash as a cement replacement agent, Journal of the American Ceramic Society 100(10) (2017) 4785-4800.
[29] D.D.W. Fowler, Characterizing Fly Ash, Center for Transportation Research (2013).
[30] Y. Abualrous, Characterization of Indian and Canadian Fly Ash for Use
in Concrete, PhD Thesis. University of Toronto (2017).
[31] A. Saraber, Fly ash from coal and biomass for use in concrete Origin, properties and performance, (2017).
[32] K.L. Aughenbaugh, T. Williamson, M.C.G. Juenger, Critical evaluation of strength prediction methods for alkali-activated fly ash, Materials and Structures 48(3) (2014) 607-620.
[33] C.R. Sheare, The Productive Reuse of Coal, Biomass and Co-fired Fly Ash, (2014).
[34] P.T. Durdziński, M. Ben Haha, S.A. Bernal, N. De Belie, E. Gruyaert, B. Lothenbach, E. Menéndez Méndez, J.L. Provis, A. Schöler, C. Stabler, Z. Tan, Y. Villagrán Zaccardi, A. Vollpracht, F. Winnefeld, M. Zając, K.L. Scrivener, Outcomes of the RILEM round robin on degree of reaction of slag and fly ash in blended cements, Materials and Structures 50(2) (2017).
[35] A.K. Mukhopadhyay, K.-W. Liu, M. Jalal, An Innovative Approach to Fly Ash Characterization and Evaluation to Prevent Alkali-Silica Reaction, ACI Materials Journal 116(4) (2019).
[36] G.B. Singh., K. Subramaniam, Characterization of Indian fly ashes using different Experimental Techniques, Indian Concrete Journal (2018).
[37] N. Moreno, X. Querol, J. Andres, K. Stanton, M. Towler, H. Nugteren, M. Janssenjurkovicova, R. Jones, Physico-chemical characteristics of European pulverized coal combustion fly ashes, Fuel 84(11) (2005) 1351-1363.
[38] B. Kim, Y.-E. Heo, C.-M. Chon, S.-J. Lee, Influence of Na/Al Ratio and Curing Temperature of

Geopolymers on Efflorescence Reduction, Resources Recycling 27(6) (2018).
[39] N.-H. Kang, C.-M. Chon, H.-T. Jou, S. Lee, Effect of Particle Size and Unburned Carbon Content of Fly Ash from Hadong Power Plant on Compressive Strength of Geopolymers, Korean Journal of Materials Research 23(9) (2013) 510-516.
[40] Y.-H. Cho, E.-M. An, C.-M. Chon, S. Lee, Effect of Fillers on High Temperature Shrinkage Reduction of Geopolymers, Journal of the Korean Institute of Resources Recycling 25(6) (2016) 73-81.
[41] Y.-H. Cho, E.-M. An, S.-J. Lee, C.-M. Chon, D.-J. Kim, Influence of Fine Aggregate Properties on Unhardened Geopolymer Concrete, Journal of the Korean Recycled Construction Resources Institute 4(2) (2016) 101-111.
[42] D. Jeon, Y. Jun, Y. Jeong, J.E. Oh, Microstructural and strength improvements through the use of Na 2 CO 3 in a cementless Ca(OH) 2 -activated Class F fly ash system, Cement and Concrete Research 67 (2015) 215-225.
[43] D. Jeon, W.S. Yum, Y. Jeong, J.E. Oh, Properties of quicklime(CaO)-activated Class F fly ash with the use of CaCl2, Cement and Concrete Research 111 (2018) 147-156.
[44] Y.K. Cho, S.H. Jung, Y.C. Choi, Effects of chemical composition of fly ash on compressive strength of fly ash cement mortar, Construction and Building Materials 204 (2019) 255-264.
[45] J.G. Jang, H.K. Lee, Effect of fly ash characteristics on delayed high-strength development of geopolymers, Construction and Building Materials 102 (2016) 260-269.
[46] J.E. Oh, Y. Jun, Y. Jeong, Characterization of geopolymers from compositionally and physically different Class F fly ashes, Cement and Concrete Composites 50 (2014) 16-26.
[47] J.E. Oh, Y. Jun, Y. Jeong, P.J.M. Monteiro, The importance of the network-modifying element content in fly ash as a simple measure to predict its strength potential for alkali-activation, Cement and Concrete Composites 57 (2015) 44-54.
[48] J.-I. Suh, W.S. Yum, H. Song, H.-G. Park, J.E. Oh, Influence of calcium nitrate and sodium nitrate on strength development and properties in quicklime(CaO)-activated Class F fly ash system, Materials and Structures 52(6) (2019).
[49] S. Jung-Il, W.S. Yum, S. Sim, H.-G. Park, J.E. Oh, Effect of magnesium formate as compared with magnesium oxide on the strength enhancement and microstructures of CaO-activated Class F fly ash system, Construction and Building Materials 253 (2020).
[50] G.D. Moon, S. Oh, Y.C. Choi, Effects of the physicochemical properties of fly ash on the compressive strength of high-volume fly

ash mortar, Construction and Building Materials 124 (2016) 1072-1080.
[51] B. Park, Y.C. Choi, Prediction of Self-Healing Potential of Cementitious Materials Incorporating Crystalline Admixture by Isothermal Calorimetry, International Journal of Concrete Structures and Materials 13(1) (2019).
[52] Y. Kim, K. Kim, G.-Y. Jeong, Study of detailed geochemistry of hazardous elements in weathered coal ashes, Fuel 193 (2017) 343-350.
[53] W.H. Zachariasen, The Atomic Arrangement in Glass, Journal of the American Chemical Society (1932) 3841-3851.
[54] S. Diamond, On the glass present in low-calcium and in high-calcium flyashes, Cement and Concrete Research 13(4) (1983) 459-464.
[55] T. Matias, F. Souza, R. Araújo, C.H. Antunes, Learning of a single-hidden layer feedforward neural network using an optimized extreme learning machine, Neurocomputing 129 (2014) 428-436.
[56] N. Tangri, D. Ansell, D. Naimark, Predicting technique survival in peritoneal dialysis patients: comparing artificial neural networks and logistic regression, Nephrol Dial Transplant 23(9) (2008) 2972-81.
[57] A.G. Schocken S, Neural Networks for Decision Support Systems: Problems and Opportunities., New York: Center for Research on Information Systems, Stern School of Business, New York University (1991).
[58] B.E. Geman S., Doursat R., Neural networks and the bias/variance dilemma, Neural Computation 4(1) (1992) 1-58.
[59] D. S., The bias-variance tradeoff: How data science can inform educational debates, AERA Open (2020).
[60] R.E.-Y. P Derbeko, R Meir, Variance optimized bagging, European Conference on Machine Learning (2022) 60-72.
[61] B.Y. Schwenk H., Boosting Neural Networks Neural Computation 12(8) (2000) 1869-1887.
[62] W.D. H., Stacked generalization, Neural Networks 5(2) (1992) 241-259.
[63] B. L., Stacked regressions, Machine Learning 24(1) (1996) 49-64.
[64] X. Yang, Y. Wang, R. Byrne, G. Schneider, S. Yang, Concepts of Artificial Intelligence for Computer-Assisted Drug Discovery, Chem Rev 119(18) (2019) 10520-10594.
[65] M. Heydarian, T.E. Doyle, R. Samavi, MLCM: Multi-Label Confusion Matrix, Institute of Electrical and Electronics Engineers 10 (2021) 19083 - 19095.

[66] R. Yacouby, D. Axman, Probabilistic Extension of Precision, Recall, and F1 Score for More Thorough Evaluation of Classification Models, (2020) 79–91.
[67] A.P. Barten, The coefficient of determination for regression without a constant term, The Practice of Econometrics 181–189 (1987).
[68] R.M. L Antwarg, B Shapira, L Rokach, Explaining anomalies detected by autoencoders using SHAP, arXiv preprint arXiv: 1903.02407 (2019).
[69] S.I.L. S. M. Lundberg, A unified approach to interpreting model predictions, Advances in neural information processing systems (2017) 4765-4774.

Abstract in Korean

본 연구에서는 머신러닝을 이용하여 건설 재료의 여러 가지의 중요한 특성을 성공적으로 예측하였다. 콘크리트 제조공정에서 플라이애시는 비용 절감 및 콘크리트 강도 개선을 목적으로 사용하는 대표적인 산업 부산물이다. 또한, 최근 시멘트계 재료에 탄소나노튜브를 혼입하여 자가 감지 또는 자가 가열 능력과 같은 시멘트 기반 다기능성을 실현할 수 있다. 본 논문에서는 플라이애시의 화학적 반응성을 예측하고, 탄소나노튜브의 분산성과 함량을 예측하는 머신러닝 모델을 만들었다. 이는 기존의 이론식 접근 방식과는 다른 데이터 기반의 패턴을 찾는 방식으로 문제를 해결하고자 한 것이다.

우선, 플라이애시의 반응성 예측은 플라이애시의 품질 변동성과 F급과 C급 플라이애시의 반응성 차이를 고려하여, 국내의 F급 플라이애시를 대상으로 모델을 만들었다. 결정계수 0.80의 예측성능으로 플라이애시의 화학 조성값을 통해 플라이애시의 반응성을 주로 결정하는 비정질 알루미노 실리케이트 양을 예측하였다. 해당 모델은 국내의 F급 플라이애시에 한정되지만, 본 연구는 재료의 특성 뿐만 아니라 반응성의 정량적 예측이 어려운 다양한 유형의 플라이애시와 보조 시멘트재(supplementary cementitious materials, SCMs)에 대해서 발전적으로 적용할 수 있다.

두번째로, 탄소나노튜브는 시멘트 복합체에서의 분산성과 재료의 함량에 따라 콘크리트 강도를 개선할 수도 있고 악화할 수 있다. 또한, 탄소나노튜브는 시멘트 기반 복합체내에서 의도된 다기능을 모두 실현할 수 없다. 탄소나노튜브가 혼입된 콘크리트의 품질을 비파괴적으로 평가하기 위해서 컴퓨터 비전을 활용한 머신러닝 모델을 만들었다. 탄소나노튜브의 초음파 처리 여부와 그 양에 대한 예측 정확도는 각각

0.92, 0.89로 매우 높다. 해당 모델은 탄소나노튜브가 혼입된 시멘트 복합체의 품질을 비파괴적으로 평가할 수 있다는 점에서 실무적인 의의가 있다. 예를 들어, 쉽게 구비할 수 있는 광학 현미경 이미지를 통해서 콘크리트 표면의 탄소나노튜브의 분산성과 함량을 높은 정확도로 예측할 수 있다. 해당 방법은 시공된 구조물의 품질 관리 방법으로써, 건설 재료의 분산성 및 함량 이외에 공극률 또는 강도와 같은 특성에 대해서도 적용이 가능하다.